

Biosynthesis of *Moringa oleifera* Phytocompounds Incorporated Silver Nanoparticles to Control the Fungal Infection

Saranya Jeyaraj¹, Ranjani Soundhararajan¹ , Hemalatha Srinivasan^{1,*} 

¹ School of Life Sciences, B. S. Abdur Rahman Crescent Institute of Science & Technology, Chennai, India

* Correspondence: hemalatha.sls@bsauniv.ac.in;

Received: 21.08.2024; Accepted: 15.07.2025; Published: 30.09.2025

Abstract: Nanotechnology is a growing research field. The novel properties of nanoparticles, including smaller size, improved solubility, surface flexibility, and versatile functionality, have opened up a crucial research field for biologists. These properties have enabled them to study complex biological functions at the scale of biomolecules. The use of natural products to synthesize nanoparticles is primarily considered since they are economical, easily available, less toxic, and highly effective. In this study, leaf extract of *Moringa oleifera* was employed to synthesize silver nanoparticles. The characterization of *Moringa oleifera* leaf extract incorporated silver nanoparticles (ML–AgNPs) was carried out by using UV/Vis absorption spectrometry, XRD, FTIR, FESEM-EDX, Zeta potential, and particle size distribution analyzer. The physicochemical properties of phytocompounds of *M. oleifera* leaves and the interaction of the phytocompounds of *M. oleifera* leaves with specific fungal proteins were also studied by *in silico* analysis. The antifungal activity of ML–AgNPs was investigated in the fungi *Lasiodiplodia theobromae* and *Mucor fragilis*. ML–AgNPs were found to curb the growth of fungal strains more efficiently than the standard antifungal agent fluconazole. The concentration of ML–AgNPs was also found to have a significant role in the growth inhibition of the tested fungal strains.

Keywords: antifungal activity; green nanotechnology; *Lasiodiplodia theobromae*; *Moringa oleifera*; *Mucor fragilis*; nanoparticles.

© 2025 by the authors. This article is an open-access article distributed under the terms and conditions of the Creative Commons Attribution (CC BY) license (<https://creativecommons.org/licenses/by/4.0/>), which permits unrestricted use, distribution, and reproduction in any medium, provided the original work is properly cited. The authors retain copyright of their work, and no permission is required from the authors or the publisher to reuse or distribute this article, as long as proper attribution is given to the original source.

1. Introduction

The occurrence of infections caused by fungal species in both humans and plants has surged globally in the past few years. Many commercially available antifungal agents have setbacks, including toxicity, high cost, low selectivity, or, conversely, a narrow spectrum of action, low rate of decomposition in the environment, environmental damage, health risks, pesticide resistance, time of action, and many more. In addition, some fungal species are more resistant to these antifungal agents due to their frequent usage. The usage of synthetic antifungal agents has raised concerns regarding environmental impacts as well as potential health risks. Hence, new antifungal agents are being developed from natural products, including medicinal plants and their various parts, such as leaves, flowers, fruits, stems, roots, seeds, and tubers. Using plants as the potential source of drug development is primarily considered because of their easy availability, abundance, safety, affordability, effectiveness, and fewer adverse effects when compared to synthetic drugs. Herbal plants have diverse chemical entities and hence provide unlimited opportunities for the discovery of many novel drug leads [1].

Nanotechnology is a rapidly growing research and development field where materials in the scale range of nanometers are being developed. Nanoparticles are particulate materials, and they have at least one dimension less than 100 nanometers (nm). The exceptional physicochemical properties, including antimicrobial, catalytic, optical, electronic, and magnetic properties of metal nanoparticles, have made them a crucial area of interest. The metal nanoparticles are usually synthesized and stabilized by chemical methods. However, in green chemistry, plants are used to synthesize nanoparticles. Green nanotechnology has drawn attention due to its advantages over synthetic and physical methods, as they are economical, environmentally safe, and can be scaled up on a large scale with ease. Green chemistry does not require toxic chemicals or high energy, temperature, and pressure [2,3]. Green nanoparticles can also be synthesized from bacteria and fungi, but they require specific culture and isolation techniques, which are not needed when plant extracts are used [4].

Moringa species are well-known medicinal plants, and each part of the plant has multiple functionalities, including its leaves being a rich source of nutrition, seeds being used in water purifiers, oils for biofuel, trunks for gum, etc [5]. Among the different *Moringa* species, the high-nutrient-containing species is *Moringa oleifera*, also called “Miracle Tree”. They are known for their antimicrobial, anti-diabetic, anticancer, antioxidant, and anti-inflammatory properties [6]. *M. oleifera* is rich in active phytochemicals, which can serve as capping and stabilizing agents in metal NPs. Almost all parts of the plant can be used, including stem, leaves, root, etc., for AgNP synthesis by using the green nanotechnology approach [7].

Endophytes are usually defined by their ability to coexist with their hosts without causing any infections to them. Many endophytes exhibit pathogenicity in the latent stage. The pathogenic shift is either due to the reduction of the tolerance of the hosts or stimulation of the hosts to exhibit aggressive behavior by the latent pathogens. These changes in the host susceptibility are mainly due to different plant stresses, and genetic factors also play an essential role in this pathogenic shift. *Lasiodiplodia theobromae* and *Mucor fragilis* are known to cause diseases in humans and plants [8].

From the family of Botryosphaeriaceae, *Lasiodiplodia theobromae* is an ascomycete fungus belonging to the class Dothideomycetes and order Botryosphaeriales. It is one of the most commonly found species of this family, particularly in tropical and subtropical regions. *L. theobromae* is an endophytic fungus and also a non-host-specific plant pathogen. It is reported to be associated with more than 500 diverse crops and trees, causing various diseases like canker, fruit, root rot, and dieback. It has also been reported to cause infections in humans, such as keratitis, pneumonia, sinusitis, and cutaneous lesions in both immunosuppressed and immunocompromised patients [9]. *L. theobromae* has been a causative agent for many plant diseases and is primarily referred to as a facultative wound pathogen [10].

The order Mucorales consists of 55 genera and over 260 species. These are cosmopolitan fungi comprising endophytes, saprobes, and parasites of plants, as well as human pathogens that can cause mucormycosis. However, the geographical distributions and ecological roles of many of these species are still not known. *Mucor fragilis* is an endophytic fungus and also a human and plant pathogen. Mucor species are characterized by their sporangiophores, which can be simple or branched into tong-type zygosporangia. Their colonies are fast-growing and have non-apophysate and spherical sporangia and layered sporangial walls [11].

Fluconazole is one of the most commonly used antifungal agents, and it is approved by the Food and Drug Administration (FDA). It belongs to the triazole family. The mechanism of

action of fluconazole is that it increases the permeability of cells by inhibiting the synthesis of ergosterol. Ergosterol is considered to be a primary constituent of the outer membrane of the fungal cell. Fluconazole inhibits the conversion of lanosterol into ergosterol by interacting with the enzyme responsible for its conversion. Fluconazole also prevents yeast formation by inhibiting endogenous respiration. Fluconazole is efficient against yeasts and other endemic fungi [12].

In this study, silver nanoparticles from *Moringa oleifera* leaf extract were synthesized and characterized. The drug likeness and physicochemical properties of phytochemicals of *M. oleifera* leaf extract and their interaction with specific proteins were also investigated through *in silico* studies. The antifungal activity of synthesized ML-AgNPs was explored in fungal strains, namely *Lasiodiplodia theobromae* and *Mucor fragilis*.

2. Materials and Methods

2.1. *In silico* studies.

2.1.1. Retrieval of structures of phytochemicals.

The various phytochemicals present in *M. oleifera* leaf were retrieved from Pubchem [4]. Swiss ADME was used to select the 29 potential phytochemicals from *M. oleifera* leaf based on their drug-likeness properties, with Lipinski violations between 0 and 2 from the website (<http://www.swissadme.ch/>). Pub Chem was applied to retrieve the structures of phytochemicals as well as the standard fluconazole in the SDF file format (<https://pubchem.ncbi.nlm.nih.gov/>) in 3D [13].

2.1.2. Protein retrieval and virtual screening.

Protein Data Bank (PDB) was used to retrieve the raw X-ray structure of the Lipase B gene (PDB ID: 7V6D) of *L. theobromae* from the website <https://www.rcsb.org/> [14]. The protein preparation for docking was done by using Discovery Studio Visualizer (BIOVIA) by removing H₂O molecules and heteroatoms, followed by the addition of polar hydrogen atoms to the selected protein molecule. PyRx version 0.8 for Windows was installed from <https://pyrx.sourceforge.io/> and used for docking studies [15]. Before the virtual screening, the input files were converted to the PDBQT file format to make them compatible with Vina Wizard docking. The protein was docked with fluconazole and 29 potential phytochemicals, and the binding energy of each interaction between protein and phytochemical was obtained. The virtual screening results were then exported as CSV files for further analysis. The protein-phytochemical interactions and their 2D diagrams were visualized using Discovery Studio Visualizer (BIOVIA) for further analysis.

2.2. *In vitro* studies.

2.2.1. Extract preparation from the leaves of *Moringa oleifera*.

Moringa oleifera is easily available and has numerous medicinal properties. The extract was prepared from the fresh leaves of *M. oleifera*. The leaves were collected, washed twice, and dried for one hour in a hot air oven at 55°C. The dried leaves were then coarsely ground. The coarsely ground powder of *M. oleifera* leaves was added to boiled distilled water and left overnight for maceration. The macerated liquid was filtered, and then centrifugation (15 min)

was carried out at 4400 RPM. Filtration was again done twice using Whatman paper to remove the fine particles. The obtained pure extract can be used for the synthesis of *Moringa oleifera* leaf extract incorporated silver nanoparticles (ML–AgNPs) [16].

2.2.2. Biosynthesis of ML–AgNPs.

The pure filtrate of the *M. oleifera* leaf extract was mixed with 1mM aqueous silver nitrate (AgNO_3) in a ratio of 1:2. In order to prevent agglomeration of nanoparticles, and it was incubated in the dark for three days at room temperature. The change in color from reddish-orange to dark brown shows that ML–AgNPs have been synthesized [17]. The reaction mixture was then dried in a water bath. The resulting dried nanoparticles were dissolved by using 30% Dimethyl sulphoxide (DMSO) and ultrasonicated for 5 minutes. The resulting colloidal suspension of ML–AgNPs was used to evaluate its antifungal potential in selected fungal strains [18].

2.2.3. Biophysical characterization of ML–AgNPs.

The formation of ML–AgNPs was confirmed by UV/Vis spectral analysis at 200–800 nm wavelengths. For UV/Vis spectral analysis, the ML–AgNPs were diluted with distilled water in the ratio 1:2. Distilled water was used as a blank. For Fourier transform infrared analysis, a 1 ml aliquot of ML–AgNPs was centrifuged (4°C) at 15,000 RPM for 20 minutes. The pellet alone was taken, discarding the supernatant. A thermostat was used to dry the pellet, and it was scanned at a $400\text{--}4000\text{ cm}^{-1}$ range to identify the functional groups associated with the ML–AgNPs. Fresh leaf extract powder was also subjected to FTIR analysis to identify the functional groups that are present in the leaf extract. The analysis of the size, morphology, and composition of ML–AgNPs was carried out by using FESEM-EDX. XRD assessed the crystallinity and structure of ML–AgNPs. The zeta potential values, along with the size distribution (particle) of ML–AgNPs, were also determined [19].

2.3. Antifungal plate assay.

The antifungal activity of ML–AgNPs was evaluated using a plate assay. The fungal strains of *Lasiodiplodia theobromae* and *Mucor fragilis* were used to investigate the antifungal activity of ML–AgNPs. They were isolated from infected leaves of *Piper nigrum* and subcultured in the Petri plates containing potato dextrose agar (PDA) medium. Each strain was grown in triplets separately in five different plates. A plate containing a PDA medium with no nanoparticles was taken as a control. A plate containing PDA medium incorporated with fluconazole was taken as a standard. Three plates were taken as tests where ML–AgNPs were incorporated into each plate containing PDA medium at different concentrations (6.25, 12.5, and $25\text{ }\mu\text{g/ml}$ ML–AgNPs, respectively). The strains were inoculated and incubated at 27°C . The radial growth of each strain was recorded daily by measuring the mycelial growth from the center of the inoculum to the extreme area of the mycelial development. When the mycelial growth reached the wall of the Petri plate, the assay was ended [20].

3. Results and Discussion

3.1. Physicochemical properties of phytochemicals of *M. oleifera* leaves.

The potential phytochemicals were selected based on their drug likeness and physicochemical properties. Swiss ADME was used to analyze the absorption, distribution, metabolism, and excretion (ADME) of phytochemicals. The compounds that satisfied the Lipinski rule of five were chosen as potential ligands for docking. The phytochemicals that satisfied the rules of Lipinski were selected as potential phytochemicals for docking. The four physicochemical parameters of Lipinski's rule of five are molecular weight < 500 Dalton, H-bond acceptors ≤ 10 , $\log P \leq 5$, and H-bond donors ≤ 5 . If a compound violates two or more of these parameters, then it would be categorized as a non-orally available drug and would have poor absorption and bioavailability [21]. From the 29 phytochemicals, 23 phytochemicals satisfied all the parameters, three phytochemicals violated one parameter, and three phytochemicals violated two parameters. All 29 phytochemicals were selected as potential ligands for docking, as their violations were between 0 and 2. All 29 phytochemicals, along with their respective IDs, formulas, molecular weights, acceptors (H), donors (H), partition coefficient values, and violation numbers, are listed in Table 1.

Table 1. Physicochemical properties of phytochemicals of *M. oleifera* and fluconazole.

S. no.	Compounds	CID	Formula	MW	Acceptors (H)	Donors (H)	Partition coefficient	# Violations
1	Fluconazole	3365	C ₁₃ H ₁₂ F ₂ N ₆ O	306.27	7	1	0.88	0
2	Quercetin	5280343	C ₁₅ H ₁₀ O ₇	302.24	7	5	1.23	0
3	Isoquercetin	5280804	C ₂₁ H ₂₀ O ₁₂	464.38	12	8	-0.25	2
4	Astragaln	5282102	C ₂₁ H ₂₀ O ₁₁	448.38	11	7	-0.25	2
5	Isorhamnetin	5281654	C ₁₆ H ₁₂ O ₇	316.26	7	4	1.65	0
6	Kaempferol	5280863	C ₁₅ H ₁₀ O ₆	286.24	6	4	1.58	0
7	Apigenin	5280443	C ₁₅ H ₁₀ O ₅	270.24	5	3	2.11	0
8	Luteolin	5280445	C ₁₅ H ₁₀ O ₆	286.24	6	4	1.73	0
9	Genistein	5280961	C ₁₅ H ₁₀ O ₅	270.24	5	3	2.04	0
10	Daidzein	5281708	C ₁₅ H ₁₀ O ₄	254.24	4	2	2.24	0
11	Myricetin	5281672	C ₁₅ H ₁₀ O ₈	318.24	8	6	0.79	1
12	Epicatechin	72276	C ₁₅ H ₁₄ O ₆	290.27	6	5	0.85	0
13	Sinabin	656568	C ₁₄ H ₁₉ NO ₁₀ S ₂	425.43	11	6	-0.94	2
14	Galic acid	370	C ₇ H ₆ O ₅	170.12	5	4	0.21	0
15	Salicylic acid	338	C ₇ H ₆ O ₃	138.12	3	2	1.24	0
16	Gentisic acid	3469	C ₇ H ₆ O ₄	154.12	4	3	0.74	0
17	Syringic acid	10742	C ₉ H ₁₀ O ₅	198.17	5	2	0.99	0
18	Ellagic acid	5281855	C ₁₄ H ₆ O ₈	302.19	8	4	1	0
19	Ferulic acid	445858	C ₁₀ H ₁₀ O ₄	194.18	4	2	1.36	0
20	Caffeic acid	689043	C ₉ H ₈ O ₄	180.16	4	3	0.93	0
21	o-Coumaric acid	637540	C ₉ H ₈ O ₃	164.16	3	2	1.4	0
22	p-Coumaric acid	637542	C ₉ H ₈ O ₃	164.16	3	2	1.26	0
23	Sinapic acid	637775	C ₁₁ H ₁₂ O ₅	224.21	5	2	1.31	0
24	Chlorogenic acid	1794427	C ₁₆ H ₁₈ O ₉	354.31	9	6	-0.38	1
25	Cryptochlorogenic acid	9798666	C ₁₆ H ₁₈ O ₉	354.31	9	6	-0.32	1
26	Niazimicin	5471459	C ₁₆ H ₂₃ NO ₆ S	357.42	6	4	0.9	0
27	Niaziminin	10023860	C ₁₈ H ₂₅ NO ₇ S	399.46	7	3	1.46	0
28	Niazirin	10426197	C ₁₆ H ₁₉ NO ₆	321.33	7	2	0.77	0
29	Vanillin	1183	C ₈ H ₈ O ₃	152.15	3	1	1.2	0
30	D-allose	439507	C ₆ H ₁₂ O ₆	180.16	6	5	-2.26	0

3.2. Molecular docking of Lipase B with phytochemicals of *M. oleifera*.

3.2.1. Interaction of Lipase B with phytochemicals of *M. oleifera*.

Molecular docking is carried out to achieve a target-ligand complex with optimized conformation and lower binding free energy. It helps to predict the practicality of any biochemical reaction before carrying out the *in vitro* and *in vivo* studies. It may provide information for drug designing by predicting the activation or inhibition of enzymes when small molecules (ligands) and protein targets interact [22]. The protein was docked against a standard antifungal agent and 29 potential phytochemicals separately. In this study, fluconazole was used as the standard antifungal agent for docking. The binding energies of each protein phytochemical interaction are listed in Table 2.

Table 2. The binding energy of protein phytochemical interaction.

S. No.	Compounds	Binding energy (kcal mol ⁻¹)	S. No.	Compounds	Binding energy (kcal mol ⁻¹)
1	Fluconazole	-7.1	16	Daidzein	-7.6
2	Astragaln	-8.6	17	Sinalbin	-7.6
3	Myricetin	-8.6	18	Caffeic acid	-7.1
4	Quercetin	-8.4	19	Niaziminin	-7
5	Luteolin	-8.3	20	Ferulic acid	-6.7
6	Chlorogenic acid	-8.2	21	o-Coumaric acid	-6.7
7	Epicatechin	-8.1	22	p-Coumaric acid	-6.6
8	Isorhamnetin	-8	23	Gallic acid	-6.2
9	Ellagic acid	-8	24	Sinapic acid	-6.2
10	Apigenin	-7.9	25	Gentisic acid	-6.1
11	Genistein	-7.9	26	Salicylic acid	-6
12	Cryptochlorogenic acid	-7.9	27	Niazirin	-6
13	Kaempferol	-7.8	28	Syringic acid	-5.9
14	Niazimicin	-7.7	29	Vanillin	-5.6
15	Isoquercetin	-7.6	30	D-allose	-5.4

3.2.2. Visualization of protein phytochemical interaction.

Virtual screening of Lipase B of *L. theobromae* (PDB ID 7V6D) with fluconazole and 29 potential phytochemicals was carried out. In plants, during pathogenesis, the lipases, extracellular enzymes, are secreted by fungal pathogens to penetrate into the barriers of the plants. These barriers help the plant defend against pathogen invasion and act as the source of signal transduction during fungal infection. The fungal pathogen counteracts this by producing hydrolytic enzymes, including lipases, which help the fungi to invade the plant tissue [23]. The interaction of Lipase B with the fluconazole (Figure 1a) and phytochemicals showed that the binding energy was lowest for Astragaln (Figure 1b) and Myricetin (Figure 1c) -8.6 kcal mol⁻¹ followed by Quercetin (Figure 1d) of -8.4 kcal mol⁻¹, Luteolin (Figure 1e) of -8.3 kcal mol⁻¹ and Chlorogenic acid (Figure 1f) of -8.2 kcal mol⁻¹. Most of the phytochemicals were found to interact with the target protein more efficiently than fluconazole. As shown in Table 2, the majority of the phytochemicals with good binding energy were found to be flavonoids, as they are well-known for their high antifungal efficacy [24].

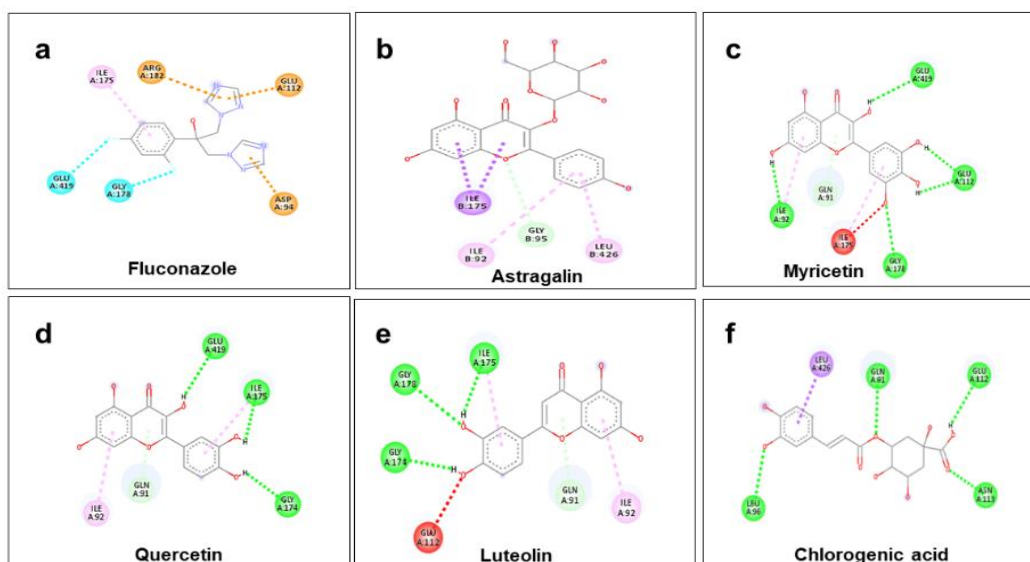


Figure 1. 2D docking images of Lipase B with (a) Fluconazole: -7.1; (b) Astragalin: -8.6 (c) Myricetin: -8.6; (d) Quercetin: -8.4; (e) Luteolin: -8.3; (f) Chlorogenic acid: -8.2 (the values are in kcal mol⁻¹)

3.3. Synthesis of ML–AgNPs.

The aqueous *M. oleifera* leaf extract was added to a 1mM silver nitrate solution to obtain *M. oleifera* incorporated silver nanoparticles. The smoky white 1 mM silver nitrate solution was mixed with the reddish-orange *M. oleifera* leaf extract, which yielded dark brown ML–AgNPs within one hour of reaction time. The color change keeps increasing with an increase in the duration of incubation in dark conditions. This is the visual confirmation for the synthesis of ML–AgNPs. The phenomenon of surface plasmon resonance of the silver metal ions, abbreviated as SPR, is the cause for the color change of the aqueous solution, as shown in Figure 2a, where the silver ions get reduced to silver nanoparticles [25].

3.4. Biophysical characterization of ML–AgNPs.

SPR results in the formation of a strong absorption band of ML–AgNPs and also the generation of color in the solution. The UV/Visible spectroscopy showed a peak of around 450 nm for ML–AgNPs, which can be seen in Figure 2b, which is in accordance with the absorbance range of silver nanoparticles. SPR peak again confirms the synthesis of ML–AgNPs [26].

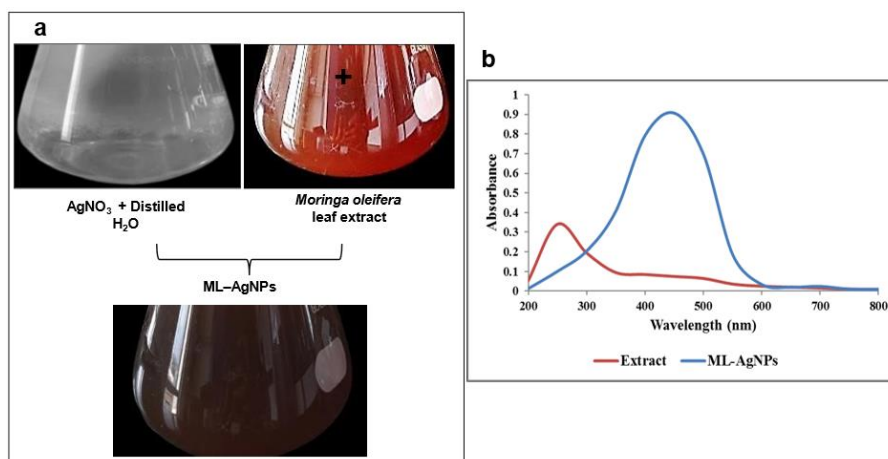


Figure 2. Synthesis and characterization of ML–AgNPs: (a) Synthesis of ML–AgNPs (dark brown) by mixing AgNO₃ solution (smoky white) with *Moringa oleifera* leaf extract (reddish orange) in the ratio 1:2 (Leaf extract: AgNO₃); (b) UV/Vis absorption spectra of *Moringa oleifera* leaf extract and ML–AgNPs.

The size, morphology, and shape of ML–AgNPs were determined using FESEM analysis. Figure 3a shows the FESEM images of ML–AgNPs at 10.00 KX magnification. The micrograph of ML–AgNPs shows different shapes with different size distributions, which indicate the presence of various phytochemicals in the *M. oleifera* leaf extract, which acted as a capping agent during the synthesis of nanoparticles [27].

The EDX spectrum of ML–AgNPs gives the elemental composition of ML–AgNPs (Figure 3b). A strong signal was observed at 3 keV, which indicates the presence of silver, which again confirms the synthesis of silver nanoparticles. The spectrum also shows the presence of Sulphur (S), Chlorine (Cl), Calcium (Ca), and Oxygen (O), which could be derived from the phytochemicals present in *M. oleifera* leaf extract. The weight percentage of Ag, O, C, Ca, S, and Cl is 39.10 %, 28.36 %, 22.25 %, 5.65 %, 2.88 %, and 1.75 %, respectively. The atom percentages of Ag, O, C, Ca, S, and Cl are 8.46 %, 41.53 %, 43.41 %, 3.30 %, 2.10 %, and 1.16 %, respectively. Results indicate that silver's weight and atom percentage are higher than those of other elements detected in EDAX analysis. These elements, Ag, O, C, Ca, S, and Cl, could play a vital role in conferring antimicrobial properties by employing a synergism mechanism in executing their action [28].

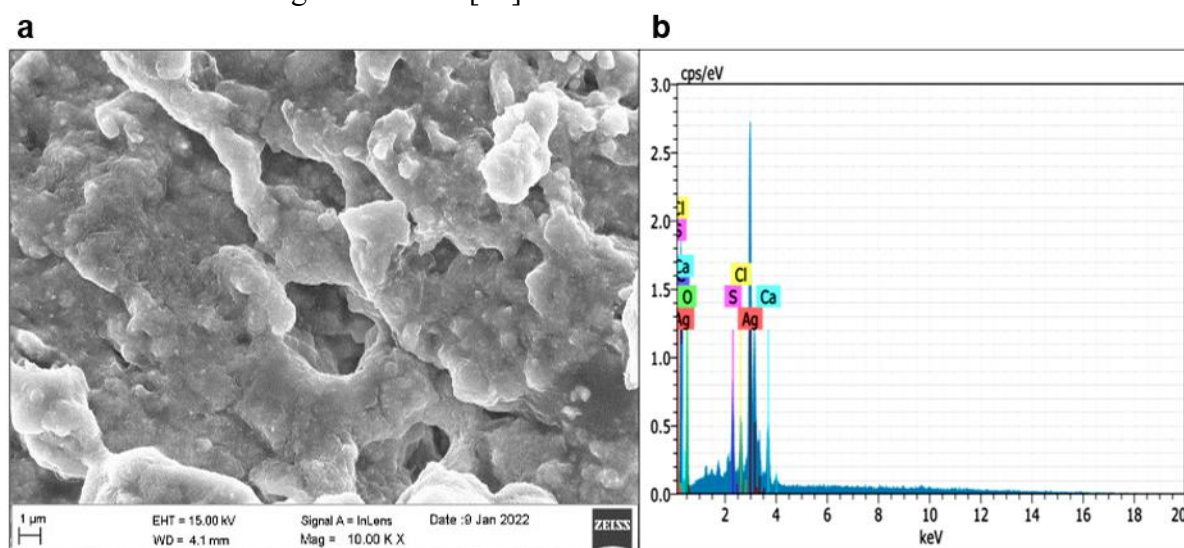


Figure 3. Characterization of ML–AgNPs: (a) FESEM image of ML–AgNPs at 10.00 KX magnification; (b) EDX spectrum of ML–AgNPs.

The technique of dynamic light scattering was employed to observe the polydispersity index (PDI), hydrodynamic size, and charge (surface) of ML–AgNPs. From Figure 4a, it is found that the size of ML–AgNPs was 667.1 nm. The PDI value was found to be in the acceptable range, that is, 0.556, which is in the midrange between 0 and 1 [29].

The zeta potential value of ML–AgNPs was -7.24mV, as shown in Figure 4b. This indicates the interaction of the biomolecules of extracts of *M. oleifera* leaf with AgNPs. ML–AgNPs' stability in the suspension is due to this repulsive force between the negatively charged AgNPs [30]. Zeta potential is a useful indicator for predicting and controlling the stability of nanoparticles. Better stability of the nanoparticles is indicated by higher zeta potential values. A zeta potential value between -30 mV and +30 mV indicates that a nanoparticle is strongly anionic or cationic, and it implies the neutrality and stability of nanoparticles in colloidal dispersion due to the presence of secondary metabolites in *M. oleifera* leaf extracts that reduce silver ions and stabilize the nanoparticles. *M. oleifera* leaf extracts contain various metabolites, including amino acids, proteins, enzymes, phytochemicals such as phenols, flavonoids, and

many more, which help to stabilize the nanoparticles during the synthesis by conferring a negative charge. The negatively charged Zeta potential helps to induce repulsion between the nanoparticles and may prevent them from aggregating. Moreover, the negative values contribute to the interaction between nanoparticles and fungal cells to exert their antifungal activity.

ML–AgNPs' crystallinity was determined by X-ray powder diffraction. Figure 4c shows the diffraction peaks at 38.21°, 45.11°, 64.35° and 77.53° of 2θ values. The crystallographic planes corresponding to these peaks are 111, 200, 220, and 311, respectively. The presence of these silver planes has been observed and compared with the standard powder diffraction card of the Joint Committee on Powder Diffraction Standards (JCPDS), silver file No. 04–0783. Based on this data, it was concluded that the crystallinity of ML–AgNPs is face-centered cubic. The other peaks in the XRD pattern could be due to the presence of phytocompounds from the leaf extract of *M. oleifera* [31].

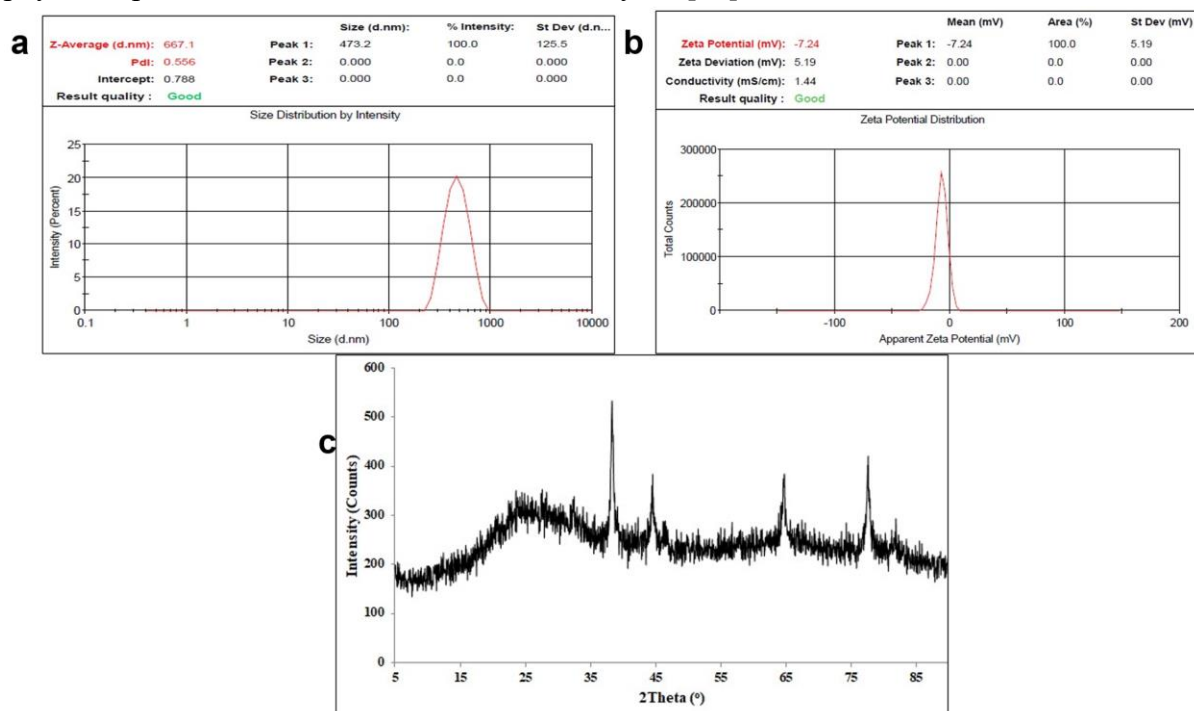


Figure 4. Characterization of ML–AgNPs: (a) Particle size distribution of ML–AgNPs obtained through DLS; (b) Zeta potential value of ML–AgNPs; (c) XRD pattern of ML–AgNPs.

The chemical composition of the *M. oleifera* leaf extract and the surface of AgNPs capped by biomolecules of *M. oleifera* leaf extract was investigated by FTIR spectroscopy. The FTIR spectrum of ML–AgNPs is shown in Figure 5a, b. Table 3 and Table 4 show the functional groups corresponding to the peak wavelengths in the spectrum, which was obtained by comparing to the standard IR spectrum table for *M. oleifera* leaf extract and ML–AgNPs. The various functional groups indicated in Tables 3 and 4 are associated with the formation and stabilization of ML–AgNPs. The FTIR footprints of Moringa extract provide the wavenumber (per cm) of 3835, 3309, 3291, 2916, 2850, 2111, 1609, 1415, and 1044, which corresponds to functional groups, namely alcohol, alcohol, alcohol, alkane, alkane, alkyne, conjugated alkene, carboxylic acid, and amine, respectively. These constituents are involved in the process where AgNO₃ is reduced into AgNPs; they also stabilize the AgNPs [32].

Table 3. Functional groups and their corresponding peak wavelengths in *M. oleifera* leaf extract.

Wave number (per cm)	Functional groups	Compound
3835	O-H Stretching	Alcohol
3309	O-H Stretching	Alcohol
3291	O-H Stretching	Alcohol
2916	C-H Stretching	Alkane
2850	C-H Stretching	Alkane
2111	C≡C Stretching	Alkyne
1609	C=C stretching	Conjugated alkene
1415	O-H bending	Carboxylic acid
1044	C-N stretching	Amine

Table 4. Functional groups and their corresponding peak wavelengths in ML–AgNPs.

Peak value (cm ⁻¹)	Functional group	Compound
3252	Hydroxyl group (OH)/Amino group (-NH ₂)	Hydroxyl group/ Amino group
2916	Alkyl group (-CH ₂ -)	Alkyl group
2308	C-N	Amide group
2112	C=C stretching	Alkyne
1994	C=O Ketene group	Ketone group
1907	Silico band (-Si-O-CH ₃)	Stretching vibration of Si-O-CH ₃
1584	N-H bending vibration	Amine
1536	Amino group NH ₂	Amino group
1393	Carboxyl group -COOH	Carboxyl group
1315	O-H bending	phenol
1194	C-O Stretch vibration	tertiary alcohol
1088	C-O-C stretch vibration	secondary alcohol
739	C-H bending	1,2-disubstituted

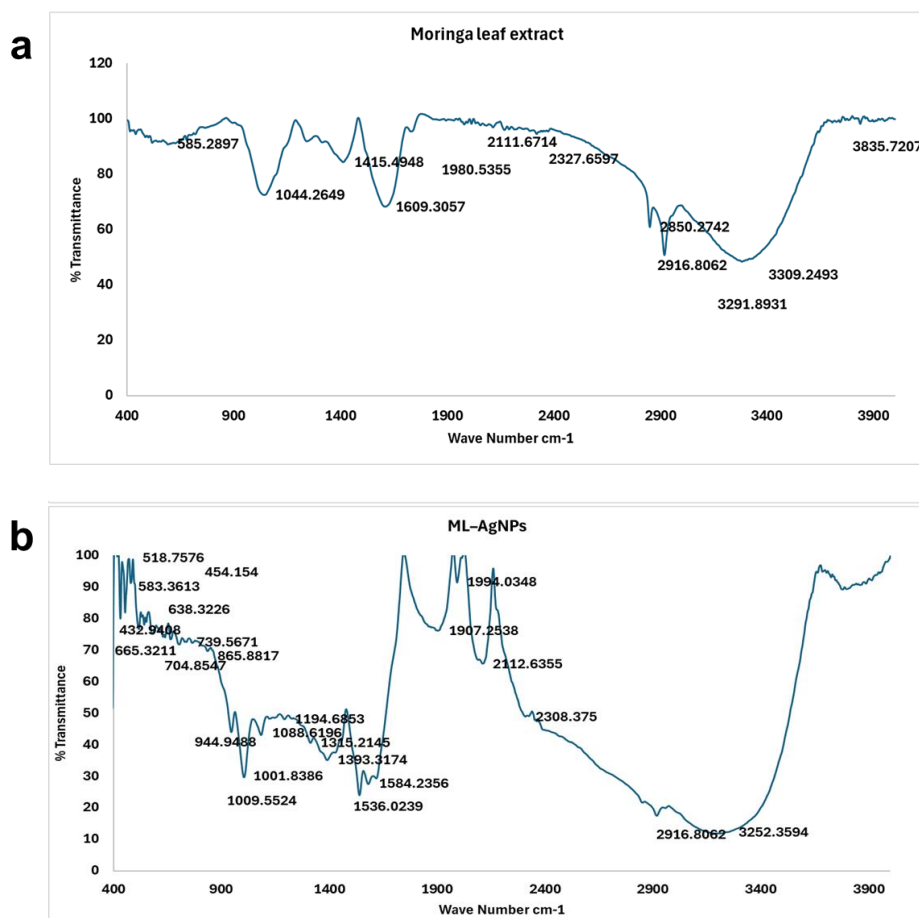


Figure 5. Characterization of ML–AgNPs: (a) FTIR spectrum of *Moringa oleifera* leaf extract; (b) FTIR spectrum of *Moringa oleifera* phytochemicals incorporated ML–AgNPs.

The FTIR footprints of ML–AgNPs provide the wavenumber (per cm) of 3252, 2916, 2308, 2112, 1994, 1907, 1584, 1536, 1393, 1315, 1194, 1088, 739, which corresponds to

functional groups, namely hydroxyl/ amino group, alkyl, amide, alkyne, ketone, stretching vibration of Si-O-CH₃, amine, amino, carboxyl, phenol, tertiary alcohol, secondary alcohol, and C-H bending of 1,2-disubstituted group respectively. The FTIR footprints confirm that the phytochemicals of *Moringa* leaves play a crucial role in the reduction of silver nitrate and in maintaining the stability of ML-AgNPs by acting as a potent capping agent.

3.5. Antifungal plate assay.

3.5.1. Radial growth assessment of *Lasiodiplodia theobromae*.

The radial growth of *Lasiodiplodia theobromae* (Figure 6a) in control (Figure 6a. A), fluconazole-treated (Figure 6a. B), and ML-AgNPs-treated PDA medium (Figure 6a. C, D, E) was observed after six days of inoculation. It was observed that the growth of *L. theobromae* was uncontrollable in the control plate. The standard antifungal agent fluconazole showed less difference when compared to the control, as it was not able to inhibit the growth of *L. theobromae* efficiently. The plates treated with ML-AgNPs showed significant differences from those of the control plate. The ML-AgNPs were found to curb the *L. theobromae* growth, and growth inhibition was significant in plates incorporated with 25 µg/ml ML-AgNPs when compared to the other two plates treated with lesser concentrations of ML-AgNPs. The color of the mycelia of *L. theobromae* started turning greyish in control and fluconazole-treated plates, which is the characteristic feature of *L. theobromae*. In ML-AgNPs plates, the color of the mycelia remained white till the end of the assay, which indicates the influence of ML-AgNPs on the morphology of *L. theobromae* [33].

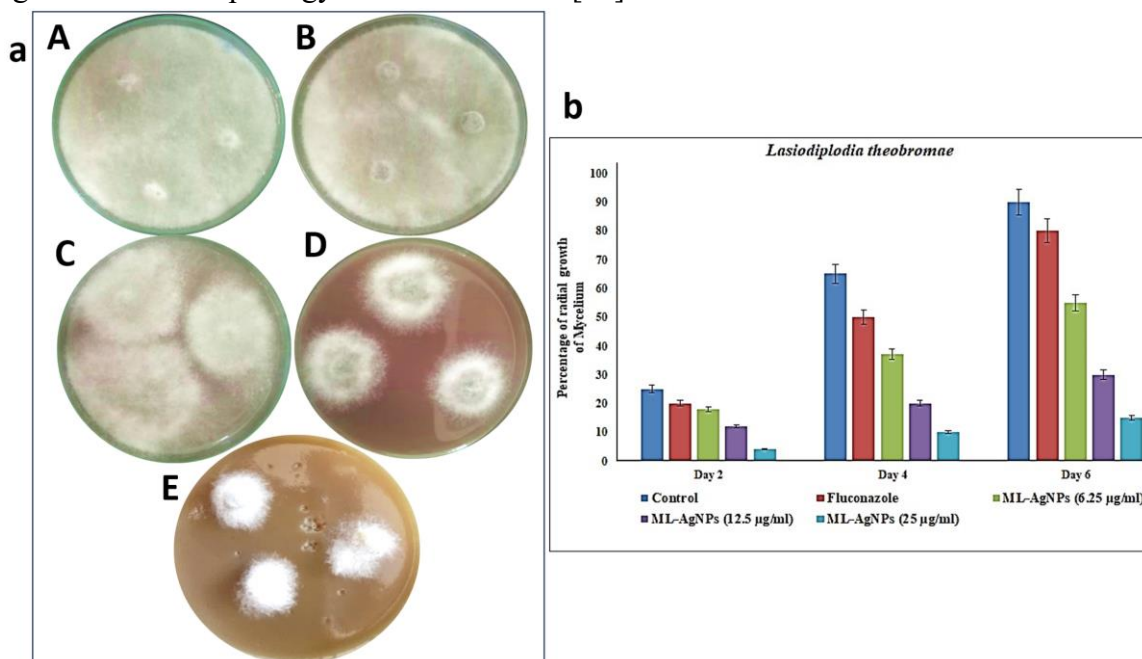


Figure 6. (a) Radial growth of *Lasiodiplodia theobromae* in A) Control; B) Fluconazole-treated medium; C) ML-AgNPs treated medium (6.25 µg/ml); D) ML-AgNPs treated medium (12.5 µg/ml); E. ML-AgNPs treated medium (25 µg/ml) observed at sixth day after inoculation; (b) Radial growth of *Lasiodiplodia theobromae* on days 2, 4 and 6 in control, fluconazole-treated medium, ML-AgNPs treated medium (6.25 µg/ml), ML-AgNPs treated medium (12.5 µg/ml) and ML-AgNPs treated medium (25 µg/ml).

The percentage of radial growth of *L. theobromae*, as observed on days 2, 4, and 6, is shown in Figure 6b [34]. The graph shows the gradual growth of *L. theobromae* for six days after inoculation. The difference between the growth of *L. theobromae* in control and ML-AgNPs-treated plates is significantly visible in this graph.

The microscopic analysis of mycelial growth of *L. theobromae* was carried out 72 hours after inoculation [35]. Not much difference was observed between the control (Figure 7a), fluconazole-treated (Figure 7b), and ML–AgNPs-treated plates (Figures 7c, 7d, 7e) in the microscopic analysis. However, the physical appearance of hyphae looks different between the control and fluconazole-treated and ML–AgNPs-treated plates.

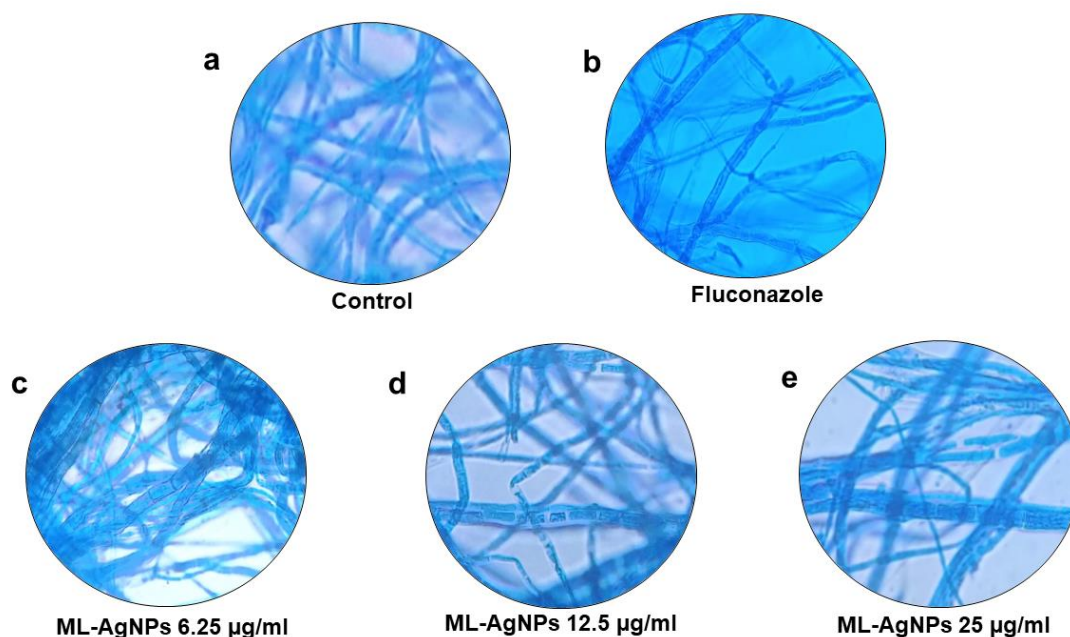


Figure 7. Microscopic analysis of mycelial growth of *Lasiodiplodia theobromae* under 40x magnification in (a) Control; (b) Fluconazole-treated medium; (c) ML–AgNPs treated medium (6.25 µg/ml); (d) ML–AgNPs treated medium (12.5 µg/ml); (e) ML–AgNPs treated medium (25 µg/ml) observed at 72 hours after inoculation

3.5.2. Radial growth assessment of *Mucor fragilis*.

The radial growth of *Mucor fragilis* in control, fluconazole-treated, and ML–AgNPs-treated PDA medium was observed after six days of inoculation. It was observed that the growth of *M. fragilis* was uncontrollable in the control plate (Figure 8a. A). Here also, the standard antifungal agent fluconazole (Figure 8a. B) showed less difference when compared to the control, as it was not able to inhibit the growth of *M. fragilis* efficiently. The plates treated with ML–AgNPs (Figure 8a. C, D, E) showed significant differences from the control plate. The ML–AgNPs were found to curb the *M. fragilis* growth, and growth inhibition was significant in plates treated with 25 µg/ml ML–AgNPs when compared to the two other plates treated with lesser concentrations of ML–AgNPs. The color of the mycelia of *M. fragilis* had turned from white to brown in control and fluconazole-treated plates, which is the characteristic feature of *M. fragilis*. In ML–AgNPs plates, the color of the mycelia remained white till the end of the assay, which indicates the influence of ML–AgNPs in the morphology of *M. fragilis* [33].

The percentage of radial growth of *M. fragilis*, as observed on days 2, 4, and 6, is shown in Figure 8b [35]. The graph shows the gradual growth of *M. fragilis* for six days after inoculation. The difference between the growth of *M. fragilis* in control and ML–AgNPs-treated plates is significantly visible in this graph.

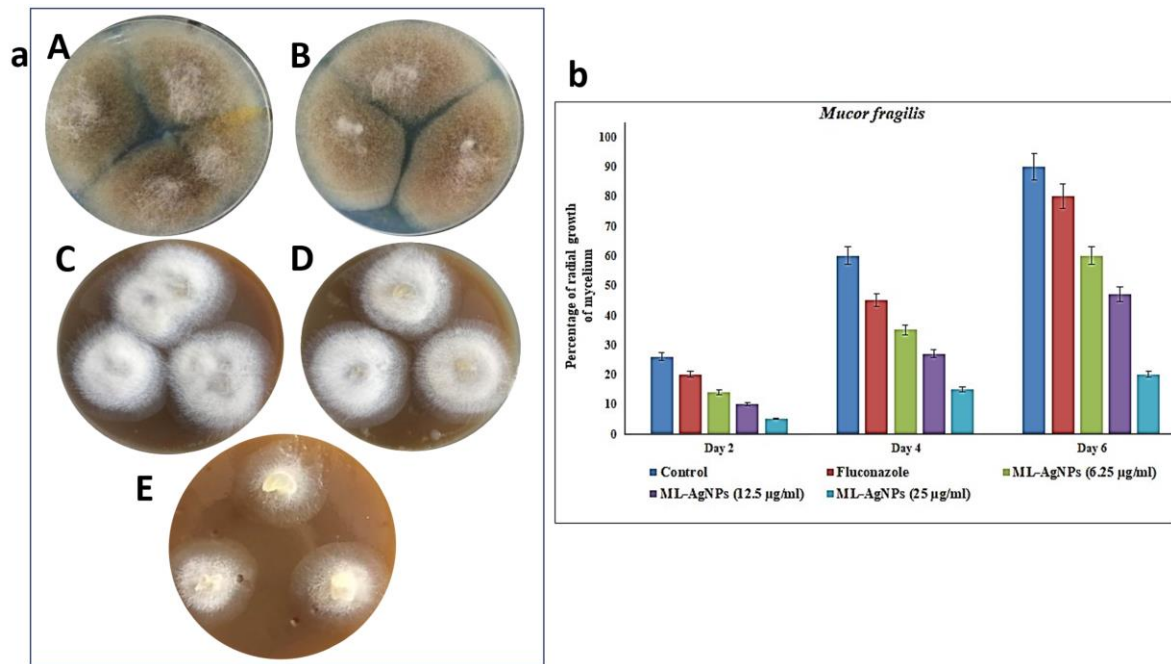


Figure 8. (a) Radial growth of *Mucor fragilis* in plate A) Control, plate; B) Fluconazole-treated medium, plate; C) ML-AgNPs treated medium (6.25 µg/ml), plate; D) ML-AgNPs treated medium (12.5 µg/ml), plate; E) ML-AgNPs treated medium (25 µg/ml) observed at sixth days after inoculation; (b) Radial growth of *Mucor fragilis* on Days 2, 4 and 6 grown in control, fluconazole-treated medium, ML-AgNPs treated medium (6.25 µg/ml), ML-AgNPs treated medium (12.5 µg/ml) and ML-AgNPs treated medium (25 µg/ml).

The microscopic analysis of mycelial growth and sporulation of *M. fragilis* was carried out 72 hours after inoculation [34]. The control plate was highly sporulated (Figure 9a). The sporulation was also significant in the fluconazole-treated plate (Figure 9b). The plates treated with ML-AgNPs (Figures 9c, 9d, 9e) showed a reduction in sporulation, and the mycelial growth was also inhibited.

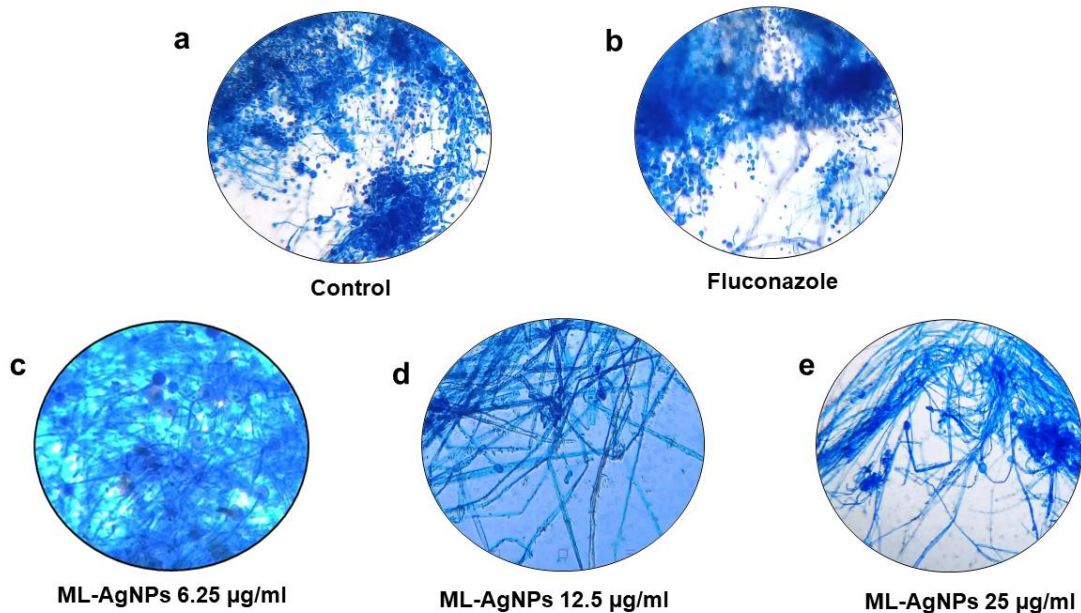


Figure 9. Microscopic analysis of mycelial growth and sporulation of *Mucor fragilis* under 10x magnification in (a) Control; (b) Fluconazole-treated medium; (c) ML-AgNPs treated medium (6.25 µg/ml); (d) ML-AgNPs treated medium (12.5 µg/ml); (e) ML-AgNPs treated medium (25 µg/ml) observed at 72 hours after inoculation.

4. Conclusions

Chemical fungicides are widely used for agricultural purposes to control fungal pathogens. Chemical fungicides are costlier and toxic to the environment, and various health risks are associated. This study has shown an effective way of controlling the pathogenic fungi, namely *Lasiodiplodia theobromae* and *Mucor fragilis*, by employing green fungicide. Green nanoparticles are better than conventional fungicides since they are safe for the ecosystem, cost-effective, efficient, non-toxic, easy to handle, bioavailable, and will not cause any secondary pollution. Hence, *Moringa oleifera* leaf extract incorporated with silver nanoparticles can be a green alternative to synthetic antifungal agents. In the near future, ML–AgNPs incorporated commercial fungicidal can be developed after validating their efficacy in field conditions and in different climatic zones. The development of nanofungicides such as nanospray will help farmers control the spread of plant fungal pathogens and protect various crops.

Author Contributions

Conceptualization, H.S.; methodology, H.S., S.J., and R.S.; software, H.S.; validation, H.S.; formal analysis, H.S., S.J., and R.S.; investigation, H.S., S.J., and R.S.; resources, H.S.; data curation, —; writing—original draft preparation, S.J. and R.S.; writing—review and editing, H.S.; visualization, H.S., S.J., and R.S.; supervision, H.S.; project administration, H.S. All authors have read and agreed to the published version of the manuscript.

Institutional Review Board Statement

Not applicable.

Informed Consent Statement

Not applicable.

Data Availability Statement

Data supporting the findings of this study are available upon reasonable request from the corresponding author.

Funding

No funding has been received for this research work.

Acknowledgments

The authors would like to thank the School of Life Sciences, B. S. Abdur Rahman Crescent Institute of Science and Technology, for providing all the facilities for the fulfillment of this research.

Conflicts of Interest

The authors declare that there is no conflict of interest.

References

1. Kamalavarshini, S.; Ranjani, S.; Hemalatha, S. Gold nanoparticles: a novel paradigm for targeted drug delivery. *Inorg. Nano-Met. Chem.* **2023**, *53*, 449–459, <https://doi.org/10.1080/24701556.2021.2025077>.
2. Asefian, S.; Ghavam, M. Green and environmentally friendly synthesis of silver nanoparticles with antibacterial properties from some medicinal plants. *BMC Biotechnol.* **2024**, *24*, 5, <https://doi.org/10.1186/s12896-023-00828-z>.
3. Górka, K.; Kubiński, K. Antifungal Activity against Human and Plant Mycopathogens, and Green Synthesis of Silver Nanoparticles Exhibiting Such Activity. *Appl. Sci.* **2024**, *14*, 115, <https://doi.org/10.3390/app14010115>.
4. Ranjani, S.; Matheen, A.; Antony Jenish, A.; Hemalatha, S. Nanotechnology derived natural poly bio-silver nanoparticles as a potential alternate biomaterial to protect against human pathogens. *Mater. Lett.* **2021**, *304*, 130555, <https://doi.org/10.1016/j.matlet.2021.130555>.
5. Jenish, A.; Ranjani, S.; Hemalatha, S. *Moringa oleifera* Nanoparticles Demonstrate Antifungal Activity Against Plant Pathogenic Fungi. *Appl. Biochem. Biotechnol.* **2022**, *194*, 4959–4970, <https://doi.org/10.1007/s12010-022-04007-2>.
6. Kashyap, P.; Kumar, S.; Riar, C.S.; Jindal, N.; Baniwal, P.; Guiné, R.P.F.; Correia, P.M.R.; Mehra, R.; Kumar, H. Recent Advances in Drumstick (*Moringa oleifera*) Leaves Bioactive Compounds: Composition, Health Benefits, Bioaccessibility, and Dietary Applications. *Antioxidants* **2022**, *11*, 402, <https://doi.org/10.3390/antiox11020402>.
7. Perumalsamy, H.; Balusamy, S.R.; Sukweenadhi, J.; Nag, S.; MubarakAli, D.; El-Agamy Farh, M.; Vijay, H.; Rahimi, S. A comprehensive review on *Moringa oleifera* nanoparticles: importance of polyphenols in nanoparticle synthesis, nanoparticle efficacy and their applications. *J. Nanobiotechnol.* **2024**, *22*, 71, <https://doi.org/10.1186/s12951-024-02332-8>.
8. Salvatore, M.M.; Andolfi, A.; Nicoletti, R. The Thin Line between Pathogenicity and Endophytism: The Case of *Lasiodiplodia theobromae*. *Agriculture* **2020**, *10*, 488, <https://doi.org/10.3390/agriculture10100488>.
9. Salvatore, M.M.; Alves, A.; Andolfi, A. Secondary Metabolites of *Lasiodiplodia theobromae*: Distribution, Chemical Diversity, Bioactivity, and Implications of Their Occurrence. *Toxins* **2020**, *12*, 457, <https://doi.org/10.3390/toxins12070457>.
10. Xing, Q.; Zhou, X.; Cao, Y.; Peng, J.; Zhang, W.; Wang, X.; Wu, J.; Li, X.; Yan, J. The woody plant-degrading pathogen *Lasiodiplodia theobromae* effector LtCrel targets the grapevine sugar-signaling protein VvRHIP1 to suppress host immunity. *J. Exp. Bot.* **2023**, *74*, 2768–2785, <https://doi.org/10.1093/jxb/erad055>.
11. Hurdeal, V.G.; Gentekaki, E.; Hyde, K.D.; Nguyen, T.T.T.; Lee, H.B. Novel *Mucor* species (Mucoromycetes, Mucoraceae) from northern Thailand. *MycKeys* **2021**, *84*, 57–78, <https://doi.org/10.3897/mycokeys.84.71530>.
12. Rasool, U.; Sah, S.K.; Hemalatha, S. EFFECT OF BIOSYNTHESIZED COPPER NANOPARTICLES (CuNPs) ON THE GROWTH AND BIOFILM FORMATION OF FLUCONAZOLE-RESISTANT CANDIDA ALBICANS. *J. Microbiol. Biotechnol. Food Sci.* **2019**, *9*, 21–24, <https://doi.org/10.15414/jmbfs.2019.9.1.21-24>.
13. Janarthanan, S.; Ranjani, S.; Hemalatha, S. Myconanoparticles Break Antibiotic Resistance in *Staphylococcus aureus* and *Acinetobacter baumannii*. *Appl. Biochem. Biotechnol.* **2023**, *195*, 196–216, <https://doi.org/10.1007/s12010-022-04125-x>.
14. Vishal, J.; Ranjani, S.; Karunya, J.R.; Hemalatha, S. Synthesis, Characterization and Evaluation of Antioxidant, Anticancer and Toxicity Properties of Silver Nanoparticles Synthesized from *Syzygium Aromaticum*. *Arch. Breast Cancer* **2023**, *10*, 291–300, <https://doi.org/10.32768/abc.2023103291-300>.
15. Mohaideen, M.S.M.H.; Srinivasan, H. Phytochemical Profiling of *Borassus flabellifer* Haustorium and its Potential Role in Combating COVID-19-Associated Encephalopathy: A Computational Perspective. *Coronaviruses* **2023**, *4*, e231023222568, <http://dx.doi.org/10.2174/0126667975267554231013112949>.
16. Ranjani, S.; Hemalatha, S. Nanoformulation target virulence genes to break antibiotic resistance in MDR *E. coli*. *Appl. Nanosci.* **2023**, *13*, 5615–5626, <https://doi.org/10.1007/s13204-023-02782-w>.
17. Khan, M.S.; Ranjani, S.; Hemalatha, S. Synthesis and characterization of *Kappaphycus alvarezii* derived silver nanoparticles and determination of antibacterial activity. *Mater. Chem. Phys* **2022**, *282*, 125985, <https://doi.org/10.1016/j.matchemphys.2022.125985>.

18. Ranjani, S.; Ahmed, M.S.; Mohd, A.; Kumar, N.S.; Ruckmani, K.; and S, H. Synthesis, characterization and applications of endophytic fungal nanoparticles. *Inorg. Nano-Met. Chem.* **2020**, *51*, 280-287, <https://doi.org/10.1080/24701556.2020.1784231>.
19. Soundhararajan, R.; Srinivasan, H. Multidrug-resistant *Bacillus species* isolated from hospital soil environment is controlled by nanobiotics incorporated nanoformulation. *Environ. Res.* **2024**, *246*, 118122, <https://doi.org/10.1016/j.envres.2024.118122>.
20. Ansari, M.; Ahmed, S.; Khan, M.T.; Hamad, N.A.; Ali, H.M.; Abbasi, A.; Mubeen, I.; Intisar, A.; Hasan, M.E.; Jasim, I.K. Evaluation of In Vitro and In Vivo Antifungal Activity of Green Synthesized Silver Nanoparticles against Early Blight in Tomato. *Horticulturae* **2023**, *9*, 369, <https://doi.org/10.3390/horticulturae9030369>.
21. Lipinski, C.A. Lead- and drug-like compounds: the rule-of-five revolution. *Drug Discov. Today Technol.* **2004**, *1*, 337–341, <https://doi.org/10.1016/j.ddtec.2004.11.007>.
22. Ragavan, M.L.; and Srinivasan, H. Therapeutic potential of dietary phytochemicals from *Drynaria quercifolia* to modulate gut microbiome: an *in silico* approach. *J. Biomol. Struct. Dyn.* **2024**, *42*, 11508–11520, <https://doi.org/10.1080/07391102.2023.2262602>.
23. Zhang, S.; Li, C.; Si, J.; Han, Z.; Chen, D. Action Mechanisms of Effectors in Plant-Pathogen Interaction. *Int. J. Mol. Sci.* **2022**, *23*, 6758, <https://doi.org/10.3390/ijms23126758>.
24. Förster, C.; Handrick, V.; Ding, Y.; Nakamura, Y.; Paetz, C.; Schneider, B.; Castro-Falcón, G.; Hughes, C.C.; Luck, K.; Poosapati, S.; Kunert, G.; Huffaker, A.; Gershenzon, J.; Schmelz, E.A.; Köllner, T.G. Biosynthesis and antifungal activity of fungus-induced *O*-methylated flavonoids in maize. *Plant Physiol.* **2022**, *188*, 167–190, <https://doi.org/10.1093/plphys/kiab496>.
25. Mittal, L.; Ranjani, S.; Ahmed, M.S.; Shree, T.J.; Tahira, A.; Poompavai, S.; G., C.I.; GowriSree, V.; Raji, S.; and S, H. Turmeric-silver-nanoparticles for effective treatment of breast cancer and to break CTX-M-15 mediated antibiotic resistance in *Escherichia coli*. *Inorg. Nano-Met. Chem.* **2021**, *51*, 867-874, <https://doi.org/10.1080/24701556.2020.1812644>.
26. Charlz Nithin, J.; Ranjani, S.; Hemalatha, S. *Mimusops elengi* Flower-Mediated Green Silver Nanoparticles Control *Staphylococcus aureus* and *Acinetobacter baumannii*. *Appl. Biochem. Biotechnol.* **2022**, *194*, 3066–3081, <https://doi.org/10.1007/s12010-022-03882-z>.
27. Soundhararajan, R.; Jenin Ravindranath, K.; Sultana Liyakath Ali, S.; Srinivasan, H. Synthesis, characterization and anti-cancerous evaluation of single clove garlic nanoparticles on Triple-Negative breast cancer cell lines. *Mater. Lett.* **2024**, *359*, 135913, <https://doi.org/10.1016/j.matlet.2024.135913>.
28. Ranjani, S.; Faridha Begum, I.; Santhoshini, J.; Senthil Kumar, N.; Ruckmani, K.; Hemalatha, S. *Mimosa pudica* floral nanoparticles: a potent antibiotic resistance breaker. *Inorg. Nano-Met. Chem.* **2021**, *51*, 1751–1758, <https://doi.org/10.1080/24701556.2020.1852429>.
29. Basheerudeen, M.A.H.; Mushtaq, S.A.; Soundhararajan, R.; Senthil Kumar, N.; Srinivasan, H. Marine endophytic fungi mediated Silver nanoparticles and their application in plant growth promotion in *Vigna radiata* L. *Int. J. Nano Dimens.* **2020**, *12*, 1–10, <https://doi.org/10.22034/ijnd.2021.676381>.
30. Soundhararajan, R.; Mohamed Sheik Meeran, S.A.F.; Prakash, S.P.; Mohammad, W.; Kandasamy, R.; Srinivasan, H. Multi potent aromatic nano colloid: synthesis, characterization and applications. *AMB Expr.* **2020**, *10*, 168, <https://doi.org/10.1186/s13568-020-01104-5>.
31. Akther, T.; Hemalatha, S. Mycosilver Nanoparticles: Synthesis, Characterization and its Efficacy against Plant Pathogenic Fungi. *BioNanoScience* **2019**, *9*, 296–301, <https://doi.org/10.1007/s12668-019-0607-y>.
32. Ranjani, S.; Hemalatha S. Triphala decorated multipotent green nanoparticles and its applications. *Mater. Lett.* **2022**, *308*, 131184, <https://doi.org/10.1016/j.matlet.2021.131184>.
33. Khuong, N.Q.; Nhien, D.B.; Thu, L.T.M.; Trong, N.D.; Hiep, P.C.; Thuan, V.M.; Quang, L.T.; Thuc, L.V.; Xuan, D.T. Using *Trichoderma asperellum* to Antagonize *Lasiodiplodia theobromae* Causing Stem-End Rot Disease on Pomelo (*Citrus maxima*). *J. Fungi* **2023**, *9*, 981, <https://doi.org/10.3390/jof9100981>.
34. Li, X.; Leng, J.; Yu, L.; Bai, H.; Li, X.; Wisniewski, M.; Liu, J.; Sui, Y. Efficacy of the biocontrol agent *Trichoderma hamatum* against *Lasiodiplodia theobromae* on macadamia. *Front. Microbiol.* **2022**, *13*, 994422, <https://doi.org/10.3389/fmicb.2022.994422>.
35. Vera-Reyes, I.; Altamirano-Hernández, J.; Reyes-de la Cruz, H.; Granados-Echegoyen, C.A.; Loera-Alvarado, G.; López-López, A.; Garcia-Cerda, L.A.; Loera-Alvarado, E. Inhibition of Phytopathogenic and Beneficial Fungi Applying Silver Nanoparticles In Vitro. *Molecules* **2022**, *27*, 8147, <https://doi.org/10.3390/molecules27238147>.

Publisher's Note & Disclaimer

The statements, opinions, and data presented in this publication are solely those of the individual author(s) and contributor(s) and do not necessarily reflect the views of the publisher and/or the editor(s). The publisher and/or the editor(s) disclaim any responsibility for the accuracy, completeness, or reliability of the content. Neither the publisher nor the editor(s) assume any legal liability for any errors, omissions, or consequences arising from the use of the information presented in this publication. Furthermore, the publisher and/or the editor(s) disclaim any liability for any injury, damage, or loss to persons or property that may result from the use of any ideas, methods, instructions, or products mentioned in the content. Readers are encouraged to independently verify any information before relying on it, and the publisher assumes no responsibility for any consequences arising from the use of materials contained in this publication.